# Single-electron transistors studied by microwave and far-infrared absorption: Theoretical results and experimental proposal

Ioan Bâldea* and Horst Köppel

*Theoretische Chemie, Physikalisch-Chemisches Institut, Universität Heidelberg, Im Neuenheimer Feld 229, D-69120 Heidelberg, Germany*

(Received 2 October 2009; revised manuscript received 30 December 2009; published 16 March 2010)

We present theoretical results on microwave and far-infrared (FIR) absorption of single-electron transistors obtained within exact numerical diagonalization for finite clusters. They show that both the microwave and the FIR spectra consist of two maxima, whose origin can be understood physically. Our results on microwave absorption provide a physically intuitive qualitative interpretation of the Kondo splitting observed by Kogan *et al.* [Science **304**, 1293 (2004)]. The present results on the FIR absorption supplement and provide a physical insight into previous results obtained by means of the numerical renormalization group. Based on our theoretical results, we propose to conduct FIR experiments to determine the charging energy and other relevant parameters.

DOI: 10.1103/PhysRevB.81.125322 PACS number(s): 85.35.Gv, 36.20.Ng, 73.23.Hk, 81.07.Ta

## I. INTRODUCTION

In a single-electron transistor (SET), which consists of a Coulomb island (or a quantum dot, QD) attached to two electrodes, a small source-drain voltage yields a current flowing only for certain values of the gate potential $V_g$.[1–4] At temperatures below the Kondo temperature ($T<T_K$), conduction occurs in a $V_g$ range delimited by the situations where the energy of the dot level $\varepsilon_d$ is such that the lowest Hubbard "band" or the highest Hubbard band is nearly resonant with the electrode Fermi energy $\varepsilon_F$, $\varepsilon_d \approx \varepsilon_F$, and $\varepsilon_d+U \approx \varepsilon_F$, respectively. Here, $U$ represents the dot charging energy, i.e., the energy required to add an extra electron on the dot. The zero-bias conductance $G$ reaches the unitary limit $G=G_0=2e^2/h$ within the Kondo plateau, which is defined by $\varepsilon_F-U \lesssim \varepsilon_d \lesssim \varepsilon_F$.

The charging energy represents a key parameter for SETs. The unpleasant fact is that $U$ cannot be directly determined from the dc zero-bias conductance; the dot energy $\varepsilon_d$ cannot be directly controlled, but rather indirectly via the potential of a gate potential $V_g$, on which it linearly depends: $\varepsilon_d=\alpha V_g+\text{const}$. If $V_{g,l}$ and $V_{g,u}$ denote the gate potentials whereat the lower and upper Hubbard bands become resonant, one gets $U=\alpha(V_{g,l}-V_{g,u})$. To determine $U$, in addition to the difference $V_{g,l}-V_{g,u}$, which is available from the transport data, supplementary hypotheses are needed to deduce the conversion factor $\alpha$, which, although physically plausible, cannot be fully justified at the nanoscale and require assumptions or arguable extrapolations of macroscopic relations to the nanoscale. One way is to assume a certain phenomenological $T$ dependence (convolution of a Lorentzian with the derivative of the Fermi function) and to fit the width of the Coulomb-blockade peaks $G(T)$.[3,5] Another possibility is to resort to the capacitance model, which describes the SET in terms of three effective capacities $C_g$, $C_s$, and $C_d$ between the dot and the gate, source, and drain, respectively.[6–8] The conversion factor, expressed by $\alpha=C_g/C(C\equiv C_g+C_s+C_d)$, can then be obtained from the Coulomb diamonds of the stability diagram. Even without inquiring whether such assumptions are justified, the inaccuracies of the parameters estimated in this way are rather large; uncertainties can be as large as $\sim 20\%$.[9] Utilizing more accurate or at least alternative methods of investigation is highly desirable.

It is a main goal of this paper to show that the far-infrared (FIR) absorption represents a possible alternative technique for the characterization of SETs and how such experiments can be conducted.

The remaining part of this paper is organized in the following manner. In Sec. II we expose the theoretical framework and in Sec. III present all relevant computational details. In Sec. IV, exact numerical results for the full ac absorption spectra are presented and analyzed in terms of a few physically relevant many-electron states. Section V is devoted to finite-size effects. Next we discuss the two distinct spectral ranges significant for SETs separately: the microwave/radio-frequency absorption in Sec. VI and the FIR absorption in Sec. VII. Experimental implications of the theoretical results for the FIR absorption are presented in Sec. VIII. Section IX is devoted to conclusions.

## II. THEORETICAL FRAMEWORK

Early studies on SETs were carried out within the so-called orthodox theory,[6,10] which treats the dot's charge and electrostatic energy as classical variables. Here, we shall use the Anderson single-impurity model, which became the standard framework to describe theoretically[11–13] and interpret experiments[3,5,7,8] in SETs, because it accounts for the quantum-mechanical nature of the electron tunneling between the Coulomb island and electrodes. The model Hamiltonian reads

$$
\begin{aligned}
H = {} & \varepsilon_F \sum_{\sigma,n=-1}^{-M_{\mathrm{L}}} a_{n,\sigma}^{\dagger} a_{n,\sigma} + \varepsilon_F \sum_{\sigma,n=1}^{M_{\mathrm{R}}} a_{n,\sigma}^{\dagger} a_{n,\sigma} \\
& - t \sum_{\sigma,n=-1}^{-M_{\mathrm{L}}+1} (a_{n,\sigma}^{\dagger} a_{n-1,\sigma} + \text{H.c.}) - t \sum_{\sigma,n=1}^{M_{\mathrm{R}}-1} (a_{n,\sigma}^{\dagger} a_{n+1,\sigma} + \text{H.c.}) \\
& - t_d \sum_{\sigma} (a_{-1,\sigma}^{\dagger} d_{\sigma} + a_{+1,\sigma}^{\dagger} d_{\sigma} + \text{H.c.}) + \varepsilon_d \sum_{\sigma} d_{\sigma}^{\dagger} d_{\sigma} \\
& + U d_{\uparrow}^{\dagger} d_{\uparrow} d_{\downarrow}^{\dagger} d_{\downarrow}. \qquad (1)
\end{aligned}
$$

 

The left (L) and right (R) electrodes are assumed to contain noninteracting electrons, which are characterized by the same bandwidth $D=4t$ and the same coupling $t_d$ to the dot. The dot is modeled by a single level, whose energy $\varepsilon_d$ can be tuned by means of a gate potential, as discussed in Sec. I. $a_{n,\sigma}(a^\dagger_{n,\sigma})$ are annihilation (creation) operators for electrons in the left and right leads (L, R) and $d_\sigma \equiv a_{0,\sigma}(d^\dagger_\sigma \equiv a^\dagger_{0,\sigma})$ destroys (creates) electrons in the QD. The number of electrons will be assumed to be equal to the number of sites, $N=M_{\rm L}+M_{\rm R}+1$.

The quantity of interest, the frequency-dependent absorption coefficient $\mu(\omega)$ in the ground state $\Psi_0$ (case of zero temperature), can be expressed as a sum of contributions of various excited states $\Psi_\lambda(H\Psi_\lambda=E_\lambda\Psi_\lambda)$

$$\mu(\omega)=\omega\sum_{\lambda\neq 0}|\langle\Psi_\lambda|P_d|\Psi_0\rangle|^2\delta(\omega-E_\lambda+E_0), \tag{2}$$

where $P_d$ is the QD dipole moment. Equation (2) represents the result of the linear-response theory by considering an ac electromagnetic perturbation $H'=-P_d\mathcal{E}_0\cos\omega t$. Various aspects of the problem of a SET in an ac field within the linear-response approximation were previously considered in several studies (see, e.g., Refs. 14–16). Because the definition of the dipole operator $P_d$ for a pointlike QD poses some problems, it is more convenient to express the matrix elements entering Eq. (2) $\langle\Psi_\lambda|P_d|\Psi_0\rangle=-i\hbar\langle\Psi_\lambda|j_d|\Psi_0\rangle/(E_\lambda-E_0)$ in terms of the current operator $j_d=(j_{-1/2}+j_{1/2})/2$, as done in similar cases,[17] which can be unambiguously defined as $j_{n+1/2}=it_n(e/\hbar)\Sigma_\sigma(a^\dagger_{n,\sigma}a_{n+1,\sigma}-\text{H.c.})$. So, the ac absorption is specified by the spectral lines λ characterized by the intensities $\mu_\lambda$ and the frequencies $\omega_\lambda$ defined by

$$\mu_\lambda=\frac{1}{\omega_\lambda}|\langle\Psi_\lambda|\hat{\tau}|\Psi_0\rangle|^2,$$

$$\hat{\tau}\equiv i\sum_\sigma(a^\dagger_{-1,\sigma}d_\sigma-a^\dagger_{+1,\sigma}d_\sigma-\text{H.c.}),$$

$$\omega_\lambda\equiv E_\lambda-E_0. \tag{3}$$

Unless otherwise specified, we shall refer throughout to a SET in the Kondo regime ($\varepsilon_F-U\lesssim\varepsilon_d\lesssim\varepsilon_F$). Moreover, we can restrict ourselves to the range $\varepsilon_F-U/2\lesssim\varepsilon_d\lesssim\varepsilon_F$ because of the particle-hole symmetry.

## III. COMPUTATIONAL DETAILS

Below, we shall present results on the ac absorption of a SET obtained by exact (Lanczos) numerical diagonalization. The method of computation we employ here is that used in our earlier works; see, e.g., Refs. 18–24. Because the full details on this method were not published and because of the significant differences between our Lanczos implementation to compute the linear response and the more familiar continued fraction algorithm,[25] we describe it below for the benefit of the reader.

In the first run, the Lanczos procedure is iterated until, after $\mathcal{N}_\mathcal{L}$ iterations, the lowest (ground state) energy $E_0$ converges. In the second run, by carrying out again $\mathcal{N}_\mathcal{L}$ iterations and with the same starting Lanczos vector, the corresponding Ritz vector $\Psi_0$ is computed by accumulation without the need of storing the Lanczos vectors. To check that this vector represents indeed the accurately evaluated ground state $\Psi_0$, we straightforwardly compute the dispersion $\langle\Psi_0|(H-E_0)^2|\Psi_0\rangle^{1/2}$ and convince ourselves that it is much smaller (usually 5–6 orders of magnitude) than the lowest excitation energy. The above scheme can also be used to reliably compute several lower excited eigenstates, but it is usually unpractical to target all the eigenstates $\Psi_\lambda$ needed to compute the linear response via Eq. (2), e.g., by orthogonalization on eigenvectors already converged in previous runs. The reason is that many eigenvectors, which are not important for the linear response, are also targeted. To ensure that the important eigenvectors are targeted, in a third Lanczos run, we employ a starting Lanczos vector adequate for the specific linear response considered. This is, in the present case, the normalized vector $P_d|\Psi_0\rangle$. The needed matrix elements $\langle\Psi_\lambda|P_d|\Psi_0\rangle$ are given by the first component of the tridiagonal vectors obtained in this third run. Usually, a number of iterations comparable to $\mathcal{N}_\mathcal{L}$ suffices for the third run. As an important test of the results for the linear response computed in this way, we always check whether they satisfy the sum rule, which can be deduced exactly from Eq. (2)

$$\sum_\lambda|\langle\Psi_\lambda|P_d|\Psi_0\rangle|^2=\langle\Psi_0|P_d^2|\Psi_0\rangle, \tag{4}$$

because the rhs is known, namely, the squared norm of the vector $P_d|\Psi_0\rangle$. In certain cases, the linear response computed within the third run does not satisfy the above sum rule, e.g., because of spurious vector duplication. Therefore, to be always on the safe side, we carry out a fourth Lanczos run, wherein, similar to the second run, we also compute and store all those Ritz vectors $\Psi_\lambda$, which where found to have a significant spectral weight $|\langle\Psi_\lambda|P_d|\Psi_0\rangle|^2$ [in practice, above $10^{-5}$ of the rhs of Eq. (4)] in the third run. Storing these vectors $\Psi_\lambda$ is not much more demanding than storing the ground state $\Psi_0$ alone, because for all the problems we investigated so far, at most ~10–20 Ritz vectors are important. The real, prohibitive limitation remains, as in all exact diagonalization approaches, the cluster size. Again, we check that these Ritz vectors are accurate eigenvectors by straightforwardly computing the dispersions $\langle\Psi_\lambda|(H-E_\lambda)^2|\Psi_\lambda\rangle^{1/2}$. By using these eigenvectors $\Psi_\lambda$ we finally compute the linear response from Eq. (2) and convince ourselves that all important eigenvectors have been targeted by checking the sum rule Eq. (4).

Proceeding in this way, the computing time is at most ~1.5–2 times larger than for implementations of the continuous fraction algorithm,[25] but we can safely rule out any numerical artifacts and have the guarantee that the solution obtained is mathematically exact. In addition and equally important, this method allows us to compute and resolve *individual* nearly degenerate spectral lines, a situation where the information that can be extracted from convoluted spectra provided by the continued fraction algorithm does not suffice. This represents a quite relevant aspect for SETs and other QD-based nanosystems, where nearly degenerate states

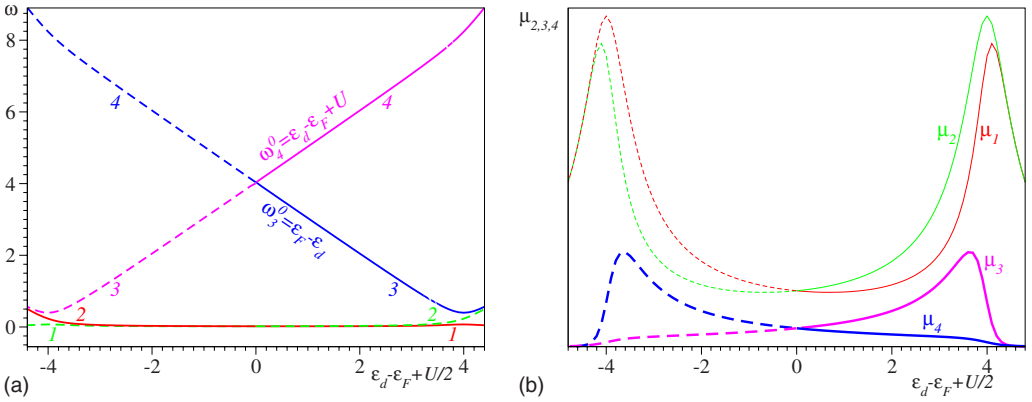


FIG. 1. (Color online) Dependence on the dot energy $\varepsilon_d$ of the four relevant (a) absorption frequencies $\omega$ (in meV) and (b) absorption intensities $\mu$ (in arbitrary units) of the optical transitions with significant spectral intensities. In (a), deeper within the Kondo plateau, the exact frequencies $\omega_{3,4}$ are well approximated by $\omega_{3,4}^0$. The dashed lines are the analytical continuations of the full lines. The parameter values are: $t=0.5$ eV, $t_d=0.2$ meV, and $U=8$ meV.

with the same symmetry (avoided crossings) are often encountered; see Refs. 22–24 and 26 and Sec. VI.

## IV. EXACT RESULTS ON THE FULL ac ABSORPTION SPECTRA AND THEIR PHYSICAL INTERPRETATION

Numerical exact results for frequencies and intensities of all the ac-absorption signals obtained as described in Sec. III are collected in Fig. 1. They have been obtained for $N=11$ and parameter values, which are typical for real cases: $t=0.5$ eV (electrode bandwidth $D=4t=2$ eV), $t_d=0.2$ meV, and $U=8$ meV. We emphasize that these are numerical exact results, obtained by using all the 213 444 multielectronic configurations of the eleven-site cluster with eleven electrons and a total spin projection $S_z=1/2$. Based on the considerations of Sec. III we can safely state that the ac spectrum of the investigated cluster solely consists of four relevant absorption signals. The other transitions, although allowed by symmetry, are completely irrelevant, as their intensities are orders of magnitude smaller and are therefore invisible in Fig. 1(b).[27]

Exact results on the SET ac absorption have of course their own importance, but do not yet provide much physical insight into the problem. Since the above exact results show that only four optical transitions are important, one can expect that, out of numerous multielectronic configurations (namely, 213 444, see above, in the case under consideration, of an eleven-site cluster with a total spin projection $S_z=1/2$), there should only exist a few many-body states, which are relevant. If so, the problem is of course to identify them and to unravel their physical content. This shall be done next.

There are nine such significant many-electron states. These configurations ($|1\rangle$ to $|9\rangle$) are schematically shown in Fig. 2. Configurations $|1\rangle$ to $|5\rangle$ correspond to one electron on the dot, in $|6\rangle$ and $|7\rangle$ the dot level is vacant, while in $|8\rangle$ and $|9\rangle$ it is occupied by two electrons. A superficial glance at the schematic representation of Fig. 2 can easily overlook both the underlying physics and the computational effort involved, and therefore a comment is in order at this point. Out of the electrons in the two electrodes, only those occupying the Fermi levels are shown for the nine states of Fig. 2. For these nine states, the single-particle states of the electrons in the electrodes are in momentum ($k$) space, and not in the real (site, $n$) space, in which the exact numerical diagonalization is carried out because the Hamiltonian matrix, Eq. (1), is sparse. A single-particle $k$ state, e.g., in the left electrode represents a superposition of $M_L$ single particle $n$ states. In addition, one should note that the electrons in electrodes depicted in Fig. 2 represent electrons at the Fermi level. This means that these electrons are delocalized over the electrodes. Consequently, although we show below that the approximative description in terms of the nine relevant states is accurate, it is not *a priori* obvious that the problem can be reduced or reasonably approximated by studying a three-site cluster. To summarize, each of the nine states depicted in Fig. 2 contains in fact numerous multielectronic configurations in the real space. However, what is physically important is the existence of a very reduced number of the relevant states.

The discussion below proceeds in terms of these nine many-body states with significant contributions to the ground state and the four excited states 1, 2, 3, and 4 depicted in Fig. 1. From these nine most relevant states one can construct the

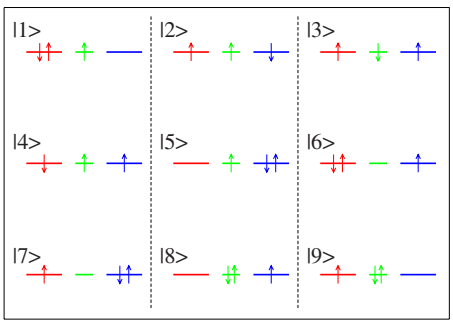


FIG. 2. (Color online) Multielectronic configurations with significant contributions to the ground state $\Psi_0$ and the excited states $\Psi_{1,2,3,4}$ important for ac absorption. For each configuration, we show the electrons at the Fermi levels of the left and right electrodes and on the dot (red, blue, and green, respectively). In either electrode, the single-electron states below the Fermi level are occupied.

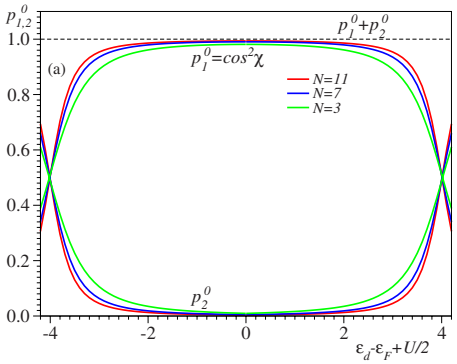


FIG. 3. (Color online) $\varepsilon_d$ dependence of the weights $p^0_{1,2}\equiv|\langle u_{1,2}|\Psi_0\rangle|^2$ of the states $u_{1,2}$ entering the linear combination of Eq. (6) for clusters with $N=3,7,11$ sites. Parameter values as in Fig. 1. For all $N$'s, the deviation from unity of the sum $p^0_1+p^0_2$ (at most $\sim 10^{-3}$) is invisible within the drawing accuracy.

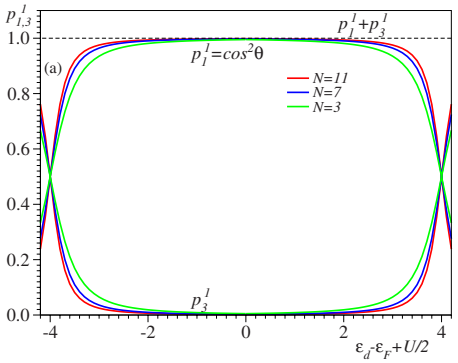


FIG. 4. (Color online) Curves for $p^1_1\equiv|\langle g_1|\Psi_1\rangle|^2$ and $p^1_3\equiv|\langle g_3|\Psi_1\rangle|^2$ similar to Fig. 3. For all $N$'s, the $p^1_1$ curve cannot be distinguished within the drawing accuracy from that for $p^3_3\equiv|\langle g_3|\Psi_3\rangle|^2$ and the $p^1_3$ curve from that for $p^3_1\equiv|\langle g_1|\Psi_3\rangle|^2$. For all $N$'s, the deviation from unity of the sum $p^1_1+p^1_3$ (at most $\sim 10^{-3}$) is invisible within the drawing accuracy.

following states with definite spin $S_z=S=1/2$ (notice that the total electron number is odd), which are either even ($g$) or odd ($u$) under space inversion

$$|u_1\rangle=(|1\rangle-|5\rangle+|2\rangle+|4\rangle-2|3\rangle)/\sqrt{8},$$

$$|u_2\rangle=(|6\rangle-|7\rangle)/\sqrt{2},$$

$$|u_3\rangle=(|8\rangle-|9\rangle)/\sqrt{2},$$

$$|g_1\rangle=(|1\rangle+|5\rangle-|2\rangle+|4\rangle)/2,$$

$$|g_2\rangle=(|1\rangle+|5\rangle+|2\rangle-|4\rangle)/2,$$

$$|g_3\rangle=(|6\rangle+|7\rangle)/\sqrt{2},$$

$$|g_4\rangle=(|8\rangle+|9\rangle)/\sqrt{2}. \quad (5)$$

The eigenstates important for ac absorption can be well approximated as

$$|\Psi_0\rangle\simeq|u_1\rangle\cos\chi-|u_2\rangle\sin\chi\rightarrow|u_1\rangle,$$

$$|\Psi_1\rangle\simeq|g_1\rangle\cos\theta-|g_3\rangle\sin\theta\rightarrow|g_1\rangle,$$

$$|\Psi_2\rangle\simeq|g_2\rangle,$$

$$|\Psi_3\rangle\simeq|g_1\rangle\sin\theta+|g_3\rangle\cos\theta\rightarrow|g_3\rangle,$$

$$|\Psi_4\rangle\simeq|g_4\rangle. \quad (6)$$

Equation (6) hold for $\varepsilon_F-U/2<\varepsilon_d<\varepsilon_F$. We can restrict ourselves to this range because of the particle-hole symmetry. For $\varepsilon_F-U<\varepsilon_d<\varepsilon_F-U/2$, the states $|6\rangle$ and $|7\rangle$ must be replaced by $|9\rangle$ and $|8\rangle$, and vice versa.

To illustrate that the eigenstates $\Psi_{0,1,2,3,4}$ computed exactly are indeed very well approximated by the expressions in the rhs of the symbols $\simeq$ in Eq. (6), we present in Figs. 3 and 4 the curves of the weights $p^0_{1,2}\equiv|\langle u_{1,2}|\Psi_0\rangle|^2$ and $p^j_i\equiv|\langle g_j|\Psi_j\rangle|^2(i,j=1,3)$. In all these cases, the two functions entering the expressions in the rhs of Eq. (6) exhaust the expansions of the exact eigenstates $\Psi_{0,1,3}$ within an accuracy of $\sim 10^{-3}$. This fact fully justifies the use of the intuitive notations in terms of cosines and sines in Eq. (6), $\cos^2\chi=p^0_1$ and $\cos^2\theta=p^1_1$. As concerns the other two exact eigenstates, the approximations $|\Psi_{2,4}\rangle\simeq|g_{2,4}\rangle$, are also accurate within $\sim 10^{-3}$.

As visible in Figs. 3 and 4, deeper within the Kondo regime, $\cos\chi\simeq 1$ and $\cos\theta\simeq 1$, and therefore $|\Psi_{0,1,3}\rangle$ are reasonably approximated as expressed in the rhs of the arrows in Eq. (6). Bearing this in mind and inspecting Eqs. (6) and (5) and Fig. 2, one can identify two groups of important eigenstates, which are well-separated energetically. The first group comprises the eigenstates $\Psi_{0,1,2}$, which basically consist of superpositions of the nearly degenerate configurations $|1\rangle-|5\rangle$, corresponding to states with a singly occupied dot. This fact nicely reveals the spin entanglement and the role of the coherent superpositions of all the possible spin-flip processes ($|1\rangle\rightleftharpoons|3\rangle$, $|3\rangle\rightleftharpoons|5\rangle$, $|2\rangle\rightleftharpoons|3\rangle$, $|4\rangle\rightleftharpoons|3\rangle$) in the formation of the nearly degenerate states $\Psi_{0,1,2}$ important for the Kondo effect. The absorption frequencies $\omega_{1,2}$ of these optical transitions are low, falling into the microwave[28] or even radio-frequency (rf) range. The second group comprises the higher energy states $\Psi_3$ and $\Psi_4$, which correspond to a dot that is either doubly occupied or empty. Loosely speaking, they amount to excite a particle-hole pair, wherein the hole state is on the dot and the particle state in electrodes, or vice versa. The corresponding absorption frequencies, $\omega_3\simeq\omega^0_3=\varepsilon_F-\varepsilon_d$ and $\omega_4\simeq\omega^0_4=\varepsilon_d+U-\varepsilon_F$ [cf. Fig. 1(a)], are on the order of the charging energy $U$, falling therefore into the FIR range.

## V. FINITE-SIZE EFFECTS

As is well known, the drastic limitation of the exact numerical diagonalization to rather small cluster sizes $N$ often precludes a reliable finite-scaling analysis. There are well-known examples (see, e.g., Refs. 19, 29, and 30) of nonmonotonic $N$-dependent properties, or qualitatively different

behaviors at smaller and larger $N$ due to a different underlying physics (see, e.g., Ref. 30) at the sizes where exact numerical diagonalization is feasible. This limitation is even more severe in the case of SETs, in the sense that not even all these small sizes can be included in a finite-scale analysis. A careful selection of the $N$ values to be included in the finite-scale analysis is often necessary, as is well known, e.g., in the case of cyclic polyenes $C_NH_N$ or related systems, where Hückel ($N=4n+2$) and anti-Hückel ($N=4n$) systems behave differently ($n$ is an integer); see, e.g., Refs. 29–31 and references cited therein. With our implementation described in Sec. III, we can reliably treat the linear response of half-filled clusters up to $N=14$, amounting to a dimension of the Hilbert space of 11 778 624. This is not too much different from the largest size ($N=12$) treated by exact diagonalization of most recent studies on the dc conductivity of model Eq. (1).[32] In view of the analysis in terms of the relevant many-body states of Fig. 2, it is clear that considering symmetric clusters (identical electrodes) is advantageous. Because short electrodes with an even number of sites are known to yield spurious results (compare Ref. 33 with Ref. 32), what remains is to consider electrodes with an odd number of sites, which mimic "metallic" electrodes (i.e., electrodes with a partially occupied Fermi level).[23,34] Concretely, this means that we are left with the values $N=3$, 7, and 11. Obviously, one cannot expect to reliably deduce a scaling law solely based on these three $N$ values.

In view of the aforementioned limitations, similar to our previous works,[23,34] we shall simply inspect whether the relevant properties computed for $N=3$, 7, and 11 are significantly size dependent or not. Typical results are shown in Figs. 3–5. They reveal that certain quantities like the lowest excitation energies $\omega_{1,2}$ of Fig. 5(b) are strongly size dependent. Obviously, such results for $\omega_{1,2}$ of exact diagonalization cannot be trusted, at least not quantitatively (see also Sec. VI).

But, similarly to the examples presented in Refs. 34 and 23, there also exist quantities, which only slightly depend on $N$. Most important for the main purpose of this work, this is the case of the two higher absorption frequencies $\omega_{3,4}$ of Fig. 5(a), the key quantities to be measured in the FIR experiments we propose here (see Sec. VIII), Therefore, to give further support to the fact why we believe that, deeper in the Kondo plateau, the results for the curves $\omega_{3,4}(\varepsilon_d)$ are not significantly affected by finite-size effects, we carried out supplementary calculations. Namely, we considered asymmetric clusters, wherein the QD is attached to the end of a single "metallic" electrode with an odd number of sites $N_u$. This procedure, which amounts to unfold the original symmetric cluster,[14,32,35] has the advantage that the size $N_u$ of the single electrode can be larger, roughly twice that of one electrode of a symmetric cluster. The largest relevant (odd) size that we can treat by exact diagonalization is $N_u=13$ (13+1 sites). The shortcoming of the asymmetric cluster is that it misses the two lowest excitations $\omega_{1,2}$ related to the coherent spin fluctuations responsible for the Kondo effect. The first excitation of the asymmetric cluster, which is almost degenerate with the singlet ground state, is a spin triplet, and the small singlet-triplet splitting could be considered as the counterpart of $\omega_{1,2}$ in symmetric clusters. However, this triplet excited state is irrelevant for the spin conserving ac-absorption processes. Most important is that the next two excitations of the asymmetric cluster are singlet states, which are optically active, and their energies are the counterpart of the above $\omega_{3,4}$. As noted in the caption of Fig. 5(a), the curves for $N_u=7$, 9, 11, and 13 cannot be distinguished from those of the symmetric cluster with $N=11$, which is the counterpart of the asymmetric cluster with $N_u=5$.

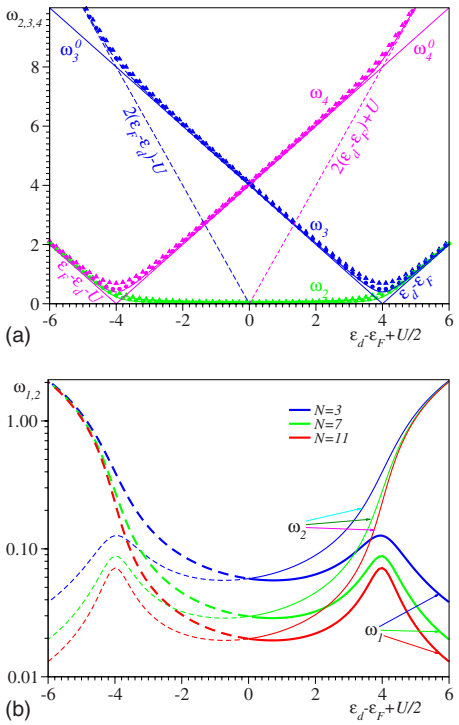


FIG. 5. (Color online) Results on the (a) higher (FIR) frequency $\omega_{3,4}$ and (b) lower (rf/microwave) frequency $\omega_{1,2}$ ac absorption for several cluster sizes $N$ and same parameter values as in Fig. 1. In panel (a), the triangles and circles are for clusters with $N=3$ and 7, respectively, and solid lines are for clusters with $N=11$. The latter cannot be distinguished within the drawing accuracy from those of asymmetric clusters, wherein the dot is attached to a single electrode with 7, 9, 11, and 13 sites. In the Kondo regime, $\omega_{3,4}$ are only slightly size dependent while $\omega_{1,2}$ are strongly size dependent. Notice the logarithmic scale on the ordinate in panel (b).

For completeness, we mention that the size dependence of $\omega_{3,4}$ remains weak even beyond the Kondo plateau (cf. Fig. 5), although this fact is not very important because of the small absorption intensities [cf. Fig. 1(b)]. There, the physical character of the $\omega_{3,4}$ excitations is different. Within the Kondo plateau they are related to excitations of a particle-hole pair, while beyond the mixed-valence points they are related to excitations of two particle-hole pairs. This becomes clear if one inspects Fig. 5(a), where the energies of the latter processes in the absence of electrode-dot coupling ($t_d \to 0$) are represented by the thin lines $2(\varepsilon_d-\varepsilon_F)+U=(\varepsilon_d-\varepsilon_F)+(\varepsilon_d+U-\varepsilon_F)$ and $2(\varepsilon_F-\varepsilon_d)-U=(\varepsilon_F-\varepsilon_d)+(\varepsilon_F-\varepsilon_d-U)$.[36] A similar change in the physical character can be seen, e.g., in the mixed-valence region between the singly occupied and the vacant dot. There, the curve $\omega_3$, which corresponds to the excitation of an electron from the singly occupied dot into electrodes

$(\omega_3 \approx \omega_3^0 = \varepsilon_F - \varepsilon_d)$, evolves into that amounting to bring an electron from electrodes to the vacant dot $(\omega_3 \approx \varepsilon_d - \varepsilon_F)$; see the lower right corner of Fig. 5(a).

By inspecting Figs. 3 and 4, one may argue that the size dependence of the wave functions $\Psi_0$, $\Psi_1$, and $\Psi_3$ is comparable; so, where does the difference between the size dependence of $\omega_{1,2}$ on one side and $\omega_{3,4}$ on the other side come from? The reason is the following. While the $\omega_{1,2}$ values are close to 0, the $\omega_{3,4}$ values vary close to the $\omega_{3,4}^0$ values, which correspond to electrode-dot excitations in the limit of vanishing electrode-dot coupling $(t_d \to 0)$, and are large $(\sim U)$ deeper within the Kondo plateau. In fact, the size dependence of the difference $\omega_{3,4} - \omega_{3,4}^0$ is comparable to that of $\omega_{1,2} - 0$, as seen in Fig. 5(a). It is the same strong $N$ dependence of $\omega_{1,2}$ that makes $\mu_{1,2}$ [cf. Eq. (3)] strongly size dependent; the matrix elements of the hopping operator $\hat{\tau}$ are nearly $N$ independent.

Although the results presented above have shown that the size dependence of the two higher optical transitions is not substantial, the important question is whether the absorption peaks $\mu_{3,4}$ survive when the cluster is linked to semi-infinite electrodes. Based on our previous investigation of photoionization[23] and on extensive calculations of the FIR absorption in broad ranges of SET parameters, we expect the following. As the size increases, the single-electron levels in electrodes become more and more dense, and the straight lines $\omega_{3,4}^0$ of Fig. 1 or Fig. 5 will intersect the numerous horizontal (i.e., $\varepsilon_d$-independent) lines corresponding to excitations of particle-hole pairs in electrodes, in a way similar to that of the energies of various ionization processes (one hole, two hole-one particle, etc) shown in Fig. 2a of Ref. 23. Similar to Ref. 23, this gives rise to a sequence of avoided crossings, but the spectral intensity remains concentrated in two diabatic states, as if these intersections were absent. From this perspective, one can also understand why, sufficiently away from the mixed-valence points, the curves for $\omega_{3,4}(\varepsilon_d)$ for the symmetric three-site cluster of Fig. 5(a) represent reasonable approximations: roughly, they correspond to one electron-hole pair excitations, wherein the state of one mate of the pair is on the dot and the other at the electrode Fermi level. For the same reason, even the asymmetric two-site cluster provides a qualitatively correct description of the FIR absorption.

As is well known,[37] a weak electrode-dot coupling yields a small broadening $(\Gamma \simeq 2t_d^2/t)$ of the isolated dot level $\varepsilon_d$. The analysis of Sec. IV indicated that, basically, each of these transitions amounts to excite an electron-hole pair. Therefore, the electrode-dot coupling should reflect itself in a small broadening of the FIR peaks centered on the values $\omega_3 \simeq \omega_3^0 = \varepsilon_F - \varepsilon_d$ and $\omega_4 \simeq \omega_4^0 = \varepsilon_d + U - \varepsilon_F$, which replace the delta-shaped $\mu_{3,4}$ lines of the finite cluster. From a strictly mathematical standpoint, to demonstrate that these FIR peaks survive when the finite cluster is linked to real electrodes, we can simply invoke their presence in the numerical renormalization-group (NRG) results,[14] which are exact and consider semi-infinite electrodes.

To end this section, we emphasize that the value $U=8$ meV used for all the numerical results presented in this paper corresponds to largest charging energy of the fabricated SETs.[39] For smaller $U$'s, the finite-size effects analyzed above are substantially weaker.

## VI. RADIO-FREQUENCY/MICROWAVE ABSORPTION

The existence of the two transitions $|\Psi_0\rangle \to |\Psi_{1,2}\rangle$ with low-absorption frequencies $\omega_{1,2}$ in the rf/microwave range is a remarkable theoretical result, because it is directly related to the recent experimental findings in SETs irradiated with microwaves.[28] At present we cannot offer a reliable quantitative analysis and must restrict ourselves to a few qualitative considerations. The first, obvious reason of this impossibility is the strong size dependence discussed in Sec. V. But there still exists another reason. As the electrodes become longer $(N \to \infty)$, we expect that $\omega_1$ tends to the Kondo resonance width $\sim T_K$. At larger $U$, this width falls off exponentially with $U$, while our exact diagonalization data exhibit a much weaker, power law decrease with $U$. This $U$ dependence is similar to that of the width in the density of states (DOS) obtained within a one-particle Green's function approach.[38] In that approach (see Ref. 32 and citations therein), the finite cluster is embedded into semi-infinite electrodes via a Dyson equation, wherein the self-energy is supposed to be not affected by electron correlations. We are not aware of similar developments for the two-particle Green's function needed for the ac absorption. Still, the aforementioned similar and (in this respect) incorrect $U$ dependence of that approach and the present one seems to signal the need for a method that (presumably approximately but accurately enough) accounts for correlations in clusters of sizes much larger than the exact diagonalization can handle. In this sense, we think that the description of Sec. IV in terms of a few relevant many-body states is useful, since it emphasizes the similarity of the lowest two frequencies $\omega_{1,2}$ to a tunnel splitting. The coherent spin fluctuations embodied into the functions $\Psi_{0,1,2}$ of Eqs. (5) and (6) amount to a coherent tunneling between configurations that are classically degenerate and have indeed similarities to the tunneling between the degenerate minima of a symmetric double-well potential. Most relevant, exponential decays of the tunnel splittings with the interaction strength are typical.[30,31] In view of the severe size limitation within exact numerical diagonalization, and because it is unlikely that the small difference between $\omega_1$ and $\omega_2$, which becomes much smaller at larger sizes, can be resolved within the density-matrix renormalization group (DMRG), we believe that the only possible approach is a semianalytical one, e.g., based on symmetry-adapted trial wave functions for the lowest states $\Psi_{0,1,2}$, which also turned out useful for other strongly correlated electron systems.[30]

To end, we believe, in spite of the above somewhat speculative considerations, that one can plausibly ascribe the excitation energy $\omega_1$ as the Kondo resonance width, while the excitation energy $\omega_2$, close to but still different from $\omega_1$, can be interpreted as the splitting of the Kondo resonance observed experimentally.[28]

## VII. FIR ABSORPTION

We shall now switch to the other two transitions $|\Psi_0\rangle \to |\Psi_{3,4}\rangle$. As seen in Fig. 1(a), the absorption frequencies $\omega_{3,4}$ are on the order of $U$. For many fabricated SETs,[2,3,39] these values belong to the FIR range. The explicit forms in Eqs. (5) and (6) show that in the Kondo regime

these two transitions amount to excite the electron from the QD lower Hubbard band (of energy $\sim\varepsilon_d$) into the electrode Fermi level and from the electrode Fermi level into the QD upper Hubbard band (of energy $\sim\varepsilon_d+U$); sufficiently away from the mixed-valence ranges ($\varepsilon_d \approx \varepsilon_F$, $\varepsilon_d \approx \varepsilon_F - U$), the exact excitation energies are well approximated by $\omega_3^0=\varepsilon_F-\varepsilon_d$ and $\omega_4^0=\varepsilon_d+U-\varepsilon_F$ [see Fig. 1(a)].

Based on Fig. 1, one expects in general two absorption peaks in FIR. In the middle of the Kondo plateau ($\varepsilon_d^*=\varepsilon_F-U/2$) the two transitions 3 and 4 are degenerate, and therefore a single peak can be observed experimentally. There, the absorption frequency is just one half of the charging energy, $\omega_3=\omega_4=\omega^* \equiv U/2$. By moving away from this point in either direction, the absorption peak splits into two peaks of different intensities located symmetrically with respect to the degenerate peak, $\omega_{3,4} \simeq \omega^* \mp |\varepsilon_d-\varepsilon_d^*|$. The farther from the symmetric point, the more pronounced is the asymmetry in intensity, the stronger is the peak $\mu_3$ at the lower frequency $\omega_3$, and the weaker the peak $\mu_4$ at the higher frequency $\omega_4$.

Out of the studies on SETs in ac fields,[14–16] excepting in part for Ref. 14, none considered the above aspects. Without establishing any relationship to the FIR absorption, the numerical results on frequency-dependent conductance deduced within the NRG of Ref. 14 show, interestingly, a weak peak (to which the authors paid little attention) for two values of $\varepsilon_d$: at $\varepsilon_d=\varepsilon_F-U$ and at $\varepsilon_d=\varepsilon_F-U/2$ (see Figs. 2 and 3, respectively, of Ref. 14, to which we refer below). This peak is directly related to our results. The situation $\varepsilon_d=\varepsilon_F-U/2$ corresponds just to the point of particle-hole symmetry, and the peak position is visible, just as predicted by the present approach, at $\omega=\omega^*$ (note that $\varepsilon_F$ is set to zero in Ref. 14). For $\varepsilon_d=\varepsilon_F-U$, the peak in Fig. 2 of Ref. 14 occurs at $\omega \sim (6\times 10^{-3}/0.025)U=0.24U$, but the authors provide no physical interpretation of this value. In excellent agreement with this value, the lower frequency peak $\mu_3$ predicted by our approach is $\omega_3=U/4$. In addition, we predict another absorption peak $\mu_4$ at a higher frequency $\omega_4=(3/4)U$ ($\omega_4/D=0.01875$ in the notation of Ref. 14), which, although in the range showed in Fig. 3, is invisible there. We can explain this fact: for the parameters of Ref. 14,[40] we estimate that the higher frequency peak would be one order of magnitude less intense than the lower frequency one. This weak intensity could hardly be distinguished in the background of the curve of Fig. 3 at $\omega/D=0.01875$. To reveal the two peaks in FIR absorption, the NRG calculations should have used situations sufficiently away from the particle-hole symmetry point ($|\varepsilon_d-\varepsilon_d^*|$ should exceed the peak widths) but still sufficiently close to it, because otherwise the high-frequency peak would be too weak and thence not visible.

Finally, we note that the two peaks in the FIR absorption at $\omega_3$ and $\omega_4$ are the counterparts of two maxima located close to the energies $\varepsilon_d$ and $\varepsilon_d+U$, which are present in the DOS along with the sharp Kondo peak (see, e.g., Fig. 3 of Ref. 41).

## VIII. EXPERIMENTAL IMPLICATIONS

Based on the above theoretical results, we propose to employ the FIR absorption as an experimental tool to characterize SETs. To avoid misunderstandings, we emphasize that the proposed experiments are different both from those carried out using rf or microwave radiation suitable for studying the Kondo resonance (e.g., Ref. 28) and from those recently proposed by us to use photoionization,[23] where photons should have energies on the order of the work function (ultraviolet radiation).

In experiments, even using a very well focused flux of FIR photons to irradiate a SET, it is important but, fortunately, easy to discriminate between absorption processes occurring in the dot and in electrodes or due to acoustic phonons. One should simply monitor absorption by varying $V_g$: the former signals are affected and should be analyzed, while the latter are not and should be disregarded. To exploit the present results, most desirable would be to record FIR absorption spectra of SETs directly. The absorption intensities may be very weak and their measurement a challenge for experimentalists. Even though difficult, this can no longer be considered a hopeless experimental task, particularly in view of the very recent advances in the field of molecular devices, enabling to measure the photon emission[42] or Raman response[43] of a *single* molecule, see Refs. 44 and 47.

## IX. CONCLUSION

Larger QDs possess smaller charging energies [e.g., $U \approx 64$ $\mu$eV (Ref. 45)], and could be investigated by rf or microwave techniques. However, smaller QDs, as those often used in a SET setup, are characterized by considerably larger charging energies [e.g., $U \approx 1.9$ meV (Ref. 3) or $U \approx 7-8$ meV (Ref. 39)], and, consequently, for them the aforementioned techniques cannot be directly employed. In the present paper, we have presented theoretical results demonstrating that FIR experiments on such SETs, which are feasible, permit to accurately determine the charging energy (and other important parameters, see Ref. 47) in a direct way. Concerning the FIR absorption, fourth aspects are worth to be mentioned.

First, one should emphasize the cross-fertilization between NRG and exact numerical diagonalization. Based on a few significant many-body configurations, the latter method is very intuitive and allowed us to give a physical content to the NRG numerical findings unraveled so far. Conversely, the agreement between the NRG results, valid for semi-infinite electrodes, and the exact diagonalization, which can be carried out only for short electrodes, demonstrates that the latter is able to make certain valuable predictions that are not affected by finite-size effects, as already noted.[23,34]

Second, we note that the investigation with the aid of FIR radiation is by no means limited to SETs. For example, in nanodevices based on double QDs, FIR absorption can also be used to deduce other relevant parameters,[46] like the inter-dot electrostatic coupling (or $V$-Hubbard strength), which are related to important properties of nanostructures (see, e.g., Refs. 22 and 24), and which cannot be straightforwardly deduced from zero-bias dc-conductance data.

Third, we emphasize that, in comparison with other methods, the FIR absorption possesses important advantages. It is not affected by parasitic currents due to unavoidable capaci-

tive couplings, as it is the case of rf or microwave techniques. Likewise, it is much less challenging than photoionization studied recently:[23] in the FIR experiments discussed in the present paper one simply needs to determine absorption energies on the order of a few millielectron volt with a reasonable accuracy, while photoionization requires the determination of ionization energies (on the order of the work functions, typically $\sim 1$ eV) with an accuracy $\sim 1$ meV.[23]

Fourth, one may ask when and why physical results obtained for finite clusters of sizes much smaller than the Kondo length $\xi_K \sim t/T_K$ are relevant. Similar to photoionization,[23] the crucial condition for the FIR absorption discussed here is a singly occupied dot ($n_d \approx 1$). It is this condition, which is satisfied for $\Gamma \lesssim \varepsilon_F - \varepsilon_d \lesssim U - \Gamma$, that allows electron transitions from the dot to electrodes and vice versa. Moreover, the dot remains singly occupied in the aforementioned $\varepsilon_d$ range even at temperatures $T$ well above the Kondo temperature $T_K$. For the FIR absorption, $T$ should only be sufficiently smaller than $\omega_{3,4} \sim U$. For SETs with $U=1.9$ meV$=22$ K,[3] $U=7-8$ meV$=81-92$ K,[39] or even $U=64$ $\mu$eV$=0.74$ K (Ref. 45) the needed temperature is much lower than that $T \ll T_K \sim 1$ mK required to observe the Kondo anomaly in zero-bias conductance data. Importantly, the charge plateaus obtained by using an isolated cluster (as used here and in Refs. 34 and 23) or a cluster embedded in semi-infinite electrodes[32,38] are very similar. For illustration, one can compare the $n_d$ curves in Fig. 6 of Ref. 34 and Fig. 1 of Ref. 23 of isolated clusters with that in Fig. 8c of Ref. 32 for an embedded cluster. The differences in $n_d$ for isolated and embedded clusters are quantitatively significant only in the mixed-valence regions ($\varepsilon_F \approx \varepsilon_d$ and $\varepsilon_F \approx \varepsilon_d + U$), but are negligible deeper into the Kondo plateau ($\Gamma \lesssim \varepsilon_F - \varepsilon_d \lesssim U - \Gamma$).[46] For excitations of a single particle-hole pair of energies $\omega_{3,4}$ on the order of $U$ (Kondo)correlations over large spatial regions $\sim \xi_K$ are not decisive. This is the physical reason why finite-size effects are not essential for the FIR absorption.

On the contrary, the rf/microwave absorption is related to the coherent superposition of spin-flip processes of energies $\sim T_K$, basically the same that are responsible for Kondo conductance. In this case, the Kondo length is important, and because it is huge for realistic SET parameters (much beyond the present DMRG capabilities), alternative methods (see Sec. VI) to the presently known numerically (almost) exact ones are necessary. In the present paper we also presented results on the SET microwave/rf absorption, which although preliminary are interesting in the context of the recent experiments revealing the splitting of the Kondo resonance.[28] We hope to return soon to this important issue, which deserves further work.

## ACKNOWLEDGMENTS

I.B. is indebted to M. Galperin for bringing Refs. 42 and 43 to his attention. The financial support provided by the Deutsche Forschungsgemeinschaft is gratefully acknowledged.

*Also at National Institute for Lasers, Plasma, and Radiation Physics, ISS, POB MG-23, RO 077125 Bucharest, Romania; ioan.baldea@pci.uni-heidelberg.de

[1] T. A. Fulton and G. J. Dolan, Phys. Rev. Lett. **59**, 109 (1987).
[2] D. Goldhaber-Gordon, H. Shtrikman, D. Mahalu, D. Abusch-Magder, U. Meirav, and M. A. Kastner, Nature (London) **391**, 156 (1998).
[3] D. Goldhaber-Gordon, J. Göres, M. A. Kastner, H. Shtrikman, D. Mahalu, and U. Meirav, Phys. Rev. Lett. **81**, 5225 (1998).
[4] W. G. van der Wiel, S. de Franceschi, T. Fujisawa, J. M. Elzerman, S. Tarucha, and L. P. Kouwenhoven, Science **289**, 2105 (2000).
[5] S. Amasha, I. J. Gelfand, M. A. Kastner, and A. Kogan, Phys. Rev. B **72**, 045308 (2005).
[6] D. V. Averin and K. K. Likharev, J. Low Temp. Phys. **62**, 345 (1986).
[7] L. P. Kouwenhoven, D. G. Austing, and S. Tarucha, Rep. Prog. Phys. **64**, 701 (2001).
[8] S. Kubatkin, A. Danilov, M. Hjort, J. Cornil, J.-L. Bredas, N. Stuhr-Hansen, P. Hedegard, and T. Bjornholm, Nature (London) **425**, 698 (2003).
[9] W. Liang, M. P. Shores, M. Bockrath, J. R. Long, and H. Park, Nature (London) **417**, 725 (2002).
[10] J. P. Pekola, K. P. Hirvi, J. P. Kauppinen, and M. A. Paalanen, Phys. Rev. Lett. **73**, 2903 (1994).
[11] T. K. Ng and P. A. Lee, Phys. Rev. Lett. **61**, 1768 (1988).
[12] L. I. Glazman and M. E. Raikh, JETP Lett. **47**, 452 (1988).
[13] W. Izumida, O. Sakai, and Y. Shimizu, J. Phys. Soc. Jpn. **67**, 2444 (1998).
[14] V. L. Campo and L. N. Oliveira, Phys. Rev. B **68**, 035337 (2003).
[15] M. Sindel, W. Hofstetter, J. von Delft, and M. Kindermann, Phys. Rev. Lett. **94**, 196602 (2005).
[16] M. A. Laakso, T. Ojanen, and T. T. Heikkilä, Phys. Rev. B **77**, 233303 (2008).
[17] R. Bozio, M. Meneghetti, and C. Pecile, Phys. Rev. B **36**, 7795 (1987).
[18] H. Köppel, W. Domcke, and L. S. Cederbaum, Adv. Chem. Phys. **57**, 59 (1984).
[19] I. Bâldea, H. Köppel, and L. S. Cederbaum, Phys. Rev. B **55**, 1481 (1997).
[20] I. Bâldea and L. S. Cederbaum, Phys. Rev. Lett. **89**, 133003 (2002).
[21] I. Bâldea and L. S. Cederbaum, Phys. Rev. B **75**, 125323 (2007).
[22] I. Bâldea and L. S. Cederbaum, Phys. Rev. B **77**, 165339 (2008).
[23] I. Bâldea and H. Köppel, Phys. Rev. B **79**, 165317 (2009).
[24] I. Bâldea, L. S. Cederbaum, and J. Schirmer, Eur. Phys. J. B **69**, 251 (2009).
[25] P. Fulde, *Electron Correlations in Molecules and Solids*, Springer Series in Solid-State Sciences Vol. 100 (Springer-Verlag, Berlin, 1991).
[26] I. Bâldea and L. S. Cederbaum, in *Handbook of Nanophysics*,

edited by K. Sattler (Taylor & Francis, Boca Raton, in press), Chap. 42.

[27] Such very weak signals could only be visible within a logarithmic scale on the ordinate, as depicted by the dots in Fig. 2 of Ref. 21, Fig. 2 of Ref. 23, or Figs. 2 and 10 of Ref. 24.

[28] A. Kogan, S. Amasha, and M. A. Kastner, Science **304**, 1293 (2004).

[29] I. Bâldea, H. Köppel, and L. S. Cederbaum, Phys. Rev. B **60**, 6646 (1999).

[30] I. Bâldea, H. Köppel, and L. S. Cederbaum, Phys. Rev. B **63**, 155308 (2001).

[31] I. Bâldea, H. Köppel, and L. S. Cederbaum, Eur. Phys. J. B **20**, 289 (2001).

[32] F. Heidrich-Meisner, G. B. Martins, C. A. Büsser, K. A. Al-Hassanieh, A. E. Feiguin, G. Chiappe, E. V. Anda, and E. Dagotto, Eur. Phys. J. B **67**, 527 (2009).

[33] C. A. Büsser, A. Moreo, and E. Dagotto, Phys. Rev. B **70**, 035402 (2004).

[34] I. Bâldea and H. Köppel, Phys. Rev. B **78**, 115315 (2008).

[35] P. Mehta and N. Andrei, Phys. Rev. Lett. **96**, 216802 (2006).

[36] In Figs. 1(a) and 5(a), the sudden slope doubling of the $\omega_3$ and $\omega_4$ curves around the mixed-valence points of coordinates $(-4,8)$ and (4, 8), respectively, result from two avoiding crossings between the curves of one-particle-one-hole and two-particle-two-hole excitations. In either case, only one mate of the two states involved in the avoided crossing is shown. The other mate (many orders of magnitude less intense), can be reconstructed by following the thin lines of Fig. 5(a).

[37] S. Datta, *Quantum Transport: Atom to Transistor* (Cambridge University Press, Cambridge, 2005).

[38] G. Chiappe and J. A. Vergés, J. Phys.: Condens. Matter **15**, 8805 (2003).

[39] H. Liu, T. Fujisawa, H. Inokawa, Y. Ono, A. Fujiwara, and Y. Hirayama, Appl. Phys. Lett. **92**, 222104 (2008).

[40] For $D=2$ eV, the charging energies in Figs. 2 and 3 of Ref. 14 are $U=50$ meV and $U=100$ meV, respectively, i.e., one or two orders of magnitude larger than for real SETs.

[41] R. Świrkowicz, J. Barnaś, and M. Wilczyński, Phys. Rev. B **68**, 195318 (2003).

[42] S. W. Wu, G. V. Nazin, and W. Ho, Phys. Rev. B **77**, 205430 (2008).

[43] D. R. Ward, N. J. Halas, J. W. Ciszek, J. M. Tour, Y. Wu, P. Nordlander, and D. Natelson, Nano Lett. **8**, 919 (2008).

[44] I. Bâldea and H. Köppel, arXiv:0905.1212 (unpublished).

[45] S. Huang, N. Fukata, M. Shimizu, T. Yamaguchi, T. Sekiguchi, and K. Ishibashi, Appl. Phys. Lett. **92**, 213110 (2008).

[46] I. Bâldea (unpublished).

[47] See supplementary material at http://link.aps.org/supplemental/10.1103/PhysRevB.81.125322 for a detailed description of how to conduct such an experiment.